Physical properties of the half-filled Hubbard model in infinite dimensions

Antoine Georges*
Laboratoire de Physique Théorique de l'Ecole Normale Supérieure, 24, rue Lhomond, 75231 Paris Cedex 05, France

Werner Krauth†
Laboratoire de Physique Statistique de l'Ecole Normale Supérieure, 24, rue Lhomond, 75231 Paris Cedex 05, France
(Received 14 September 1992; revised manuscript received 11 February 1993)

A detailed quantitative study of the physical properties of the infinite-dimensional Hubbard model at half filling is presented. The method makes use of an exact mapping onto a single-impurity model supplemented by a self-consistency condition. This coupled problem is solved numerically. Results for thermodynamic quantities (specific heat, entropy,...), one-particle spectral properties, and magnetic properties (response to a uniform magnetic field) are presented and discussed. The nature of the Mott-Hubbard metal-insulator transition found in this model is investigated. A numerical solution of the mean-field equations *inside* the antiferromagnetic phase is also reported.

I. INTRODUCTION

Strongly correlated fermion systems have been the subject of a considerable amount of work in the last few years. The cuprate superconductors and heavy-fermion materials provide outstanding physical motivation, but along the way many aspects of "older" physical systems, such as liquid ^{3}He or Mott insulators, are being discussed anew.

The difficulty of these problems is not to be found only in the absence of any obvious small parameter in the strong-coupling regime. More deeply, it is due to the difficulty of handling simultaneously *itinerant aspects* (spatial correlations) and *atomic aspects* (on-site quantum fluctuations) in a single theoretical scheme. It is the interplay of these two characters which is at the heart of the problem, especially for the regime of intermediate couplings relevant to many of the above examples.

Recently, significant advances have been made in understanding strongly correlated fermion models in the limit of *infinite spatial dimensionality* ($d \rightarrow \infty$) first investigated by Metzner and Vollhardt.[1,2] This limit has been shown[3-5] to provide a natural generalization to quantum many-body problems of the *mean-field theory*, familiar in statistical mechanics. Most importantly, it deals with itinerant and atomic aspects on an equal footing and captures their interplay. Exact "mean-field" equations for the Green's functions have been established in this limit,[6,7,3,4] which map the problem onto a *single-impurity* quantum problem supplemented by a *self-consistency* condition.[3,4] This makes the problem amenable to various analytical and numerical treatments. Most recently, three independent works have demonstrated the possibility of a full numerical solution of the $d = \infty$ Hubbard model using this mapping.[8-10]

The aim of this paper is to give a detailed and quantitative discussion of the $d = \infty$ Hubbard model at half filling, putting the emphasis on the calculation of *physical quantities* (e.g., thermodynamics, excitation spectrum,...). We use two complementary methods. The first is the (essentially exact) numerical technique of Ref. 9 that we use for the computation of imaginary-time Green's functions, thermodynamic quantities, and in order to study the response to external fields at finite temperature. The second (approximate) method is based on the iteration of a weak-coupling scheme. It was first introduced in Ref. 3 and recently elaborated upon in Ref. 11. It can be used directly at zero temperature and yields real-frequency dynamic quantities and spectral densities. The two methods are found to agree with each other in a spectacular way in phases with unbroken spin and translational symmetry, as previously observed in Ref. 11.

Besides calculating physical quantities in the paramagnetic phase of the model, we also demonstrate in this paper that the $d = \infty$ mean-field equations can be solved numerically in the antiferromagnetic phase and in the presence of an external magnetic field. The first numerical calculation of uniform and staggered magnetizations is presented using this method.

This paper is organized as follows. In Sec. II, we define the model and establish notations (Sec. II A), summarize the equations for the single-particle Green's functions with emphasis on their mean-field content (Sec. II B), and review the connection with the Anderson-Wolff model of a magnetic impurity (Sec. II C). Section III is devoted to the explanation of the methods of the solution: full numerical solution (Sec. III A) and approximation scheme based on "iterated perturbation theory" (Sec. III B). To facilitate the reading of this paper, an overview of the phase diagram and phase transitions found subsequently is given in Sec. IV. We find two equilibrium phases: a two-sublattice antiferromagnet at low temperatures, also studied in Ref. 8, and a paramagnetic phase. In addition, as reported in Refs. 9 and 10, the paramagnetic equations display an instability, which corresponds to a transition between a *paramagnetic metal* (Fermi liquid) for weak coupling and a *paramagnetic Mott-Hubbard insulator* for strong coupling.

The rest of the paper is devoted to a detailed presenta-

0163-1829/93/48(10)/7167(16)/$06.00

tion of the physical properties of each of these regimes: the paramagnetic itinerant regime in Sec. V, the Mott-Hubbard localized paramagnet in Sec. VI, and the antiferromagnetic phase in Sec. VII.

II. EXACT MEAN-FIELD PICTURE IN $D=\infty$

A. Model and notations

We consider in this paper the Hubbard model[12]

$$H=-\sum_{\langle ij\rangle\sigma} t_{ij}c_{i\sigma}^{\dagger}c_{j\sigma}+\text{H.c.}+U\sum_{i} n_{i\uparrow}n_{i\downarrow} \tag{1}$$

with nearest-neighbor hopping on a lattice of connectivity z. Two specific cases will be considered: the d-dimensional hypercubic (hc) lattice ($z=2d$) and the Bethe lattice (Cayley tree), both in the limit $z\to\infty$. In order for the kinetic and interaction energies to remain of the same order of magnitude in this limit, the hopping must be scaled[1] as $t_{ij}=t_*/\sqrt{2z}$. The free ($U=0$) density of states (DOS) $D(\epsilon)=\sum_{\mathbf{k}}\delta(\epsilon-\epsilon_{\mathbf{k}})$ then acquires the following limit forms:[1,2]

$$\text{Hypercubic lattice, } d\to\infty:\quad D(\epsilon)=\frac{1}{t_*\sqrt{\pi}}e^{-(\epsilon/t_*)^2}, \tag{2}$$

$$\text{Bethe lattice, } z\to\infty:\quad D(\epsilon)=\frac{1}{\pi t_*}\sqrt{2-(\epsilon/t_*)^2}\ . \tag{3}$$

Unless explicitly stated, we will everywhere set $t_*=1$ in the following. As a simple consequence of the central limit theorem, a Gaussian distribution is obtained on the hypercubic lattice. It is unbounded because of "exceptional" values of the momentum (such as $\mathbf{k}=0$) for which $\epsilon_{\mathbf{k}}=O(d)$. Some details of the physics depend on this feature. Note, however, that both distributions have a *finite* kinetic energy per particle ϵ_0, and in this sense a finite bandwidth [at half filling $\epsilon_0=-t_*/\sqrt{\pi}$, $=-4\sqrt{2}t_*/3\pi$ for (2) and (3) respectively].

It is also important to notice that the $1/\sqrt{z}$ scaling leads to an antiferromagnetic exchange coupling $J_{ij}\simeq t_{ij}^2/U=O(1/z)$ which is precisely such that *finite* transition temperatures (and hence, ordered phases) are kept in the $z\to\infty$ limit. Indeed the exchange energy between one site and its shell of z neighbors with opposite spins remains $O(1)$. The fact that the *individual* exchange between two given spins vanishes as $z\to\infty$ has some important physical consequences however (see, e.g., Sec. VI C).

B. Mean-field equations

We deal extensively in this paper with the single-particle Green's function, defined at finite temperature by

$$G_{ij,\sigma}(\tau-\tau')\equiv-\langle Tc_{i,\sigma}(\tau)c_{j,\sigma}^{\dagger}(\tau')\rangle\ ,$$

where the imaginary time τ runs between 0 and $\beta=1/T$. Let us consider first a phase with unbroken spin and translation invariance, and define the self-energy in the usual way [$\omega_n=(2n+1)\pi/\beta$]:

$$G(\mathbf{k},i\omega_n)=\frac{1}{i\omega_n+\mu-\epsilon_{\mathbf{k}}-\Sigma}\ . \tag{4}$$

In the limit $z=\infty$, the self-energy no longer depends on momentum: $\Sigma=\Sigma(i\omega_n)$.[13] Hence, all the information on single-particle properties is encoded in a function of frequency only. The underlying physical reason for this simplification is that the $z\to\infty$ limit freezes *spatial* fluctuations but retains the nontrivial dynamics of *temporal* on-site fluctuations between the four possible states: $|0\rangle$, $|\uparrow\rangle$, $|\downarrow\rangle$, and $|\uparrow,\downarrow\rangle$. As recently realized in several works,[7,6,3,4] it is thus possible to obtain all single-particle properties from the study of a *single-site* problem which describes the effective dynamics of these fluctuations. We follow here the formulation of Refs. 3 and 4, in which the effective action for this single-site problem is shown to be

$$\mathcal{S}=U\int_0^{\beta}d\tau\, n_{\uparrow}(\tau)n_{\downarrow}(\tau)-\int_0^{\beta}d\tau\int_0^{\beta}d\tau'\sum_{\sigma}c_{\sigma}^{\dagger}(\tau)[(\partial_{\tau}+\mu)\delta(\tau-\tau')-\mathcal{A}(\tau-\tau')]c_{\sigma}(\tau')\ . \tag{5}$$

Here, $\mathcal{A}(\tau-\tau')$ is an effective two-body amplitude which describes processes in which an electron leaves the site, wanders among the rest of the lattice, and comes back (or is replaced by another with equal spin) at a later time. $\mathcal{A}(\tau-\tau')$ depends on the processes happening on all the other sites and hence is *not known explicitly*. It is related to the interacting Green's function of $\mathcal{S}$, $G(\tau-\tau')\equiv-\langle Tc(\tau)c^{\dagger}(\tau')\rangle_{\mathcal{S}}$, by a self-consistency condition which reads

$$G(i\omega_n)=\tilde{D}[\mathcal{A}(i\omega_n)+G(i\omega_n)^{-1}]\ . \tag{6}$$

In this expression, $\tilde{D}$ denotes the Hilbert transform of $D(\epsilon)$: $\tilde{D}(z)\equiv\int_{-\infty}^{+\infty}d\epsilon D(\epsilon)/(z-\epsilon)$. A solution of the single-site problem (5) supplemented by the constraint (6) fully determines $G(i\omega_n)$ and $\mathcal{A}(i\omega_n)$ in a coupled manner. The self-energy Σ is related to this solution by

$$i\omega_n+\mu-\Sigma(i\omega_n)=\mathcal{A}(i\omega_n)+G(i\omega_n)^{-1}\ . \tag{7}$$

This identification is such that $G(i\omega_n)$ just coincides with the *site-diagonal* Green's function of the lattice model: $G(i\omega_n)=\sum_{\mathbf{k}}G(\mathbf{k},i\omega_n)$, as expressed by (6). The notations used here are slightly different from those of our previous papers,[3,4,9] in which we denoted by G_0 the function which plays the role of the "bare" Green's function in the single-site action $\mathcal{S}$:

$$G_0(i\omega_n)^{-1}\equiv i\omega_n+\mu-\mathcal{A}(i\omega_n)\ . \tag{8}$$

Whenever convenient, we shall make use of this alterna-

tive notation below [G_0 is *not to be confused* with the free ($U=0$) on-site Green's function however].

Equations (5) and (6) are *exact* for the hypercubic and Bethe lattices in the limit $z\to\infty$.[14] They have the physical content of a *mean-field theory* in which a lattice problem is reduced to a single-site problem whose dynamics is self-consistently related to the rest of the lattice which plays the role of an "external bath" for the isolated site.

Explicit expressions can be given for the Hilbert transform $\tilde{D}$ for both the Gaussian and semicircular DOS. They read

$$\tilde{D}(\zeta)=-is\sqrt{\pi}\exp(-\zeta^2)\mathrm{erfc}(-is\zeta)$$

with $s=\mathrm{sgn}(\mathrm{Im}\zeta)$ in the former and $\tilde{D}(\zeta)=\zeta-\sqrt{\zeta^2-2}$ in the latter ($t_*=1$).[15] This last expression allows one to rewrite the self-consistency condition (6) for the Bethe lattice in a much simpler form:

$$\text{Bethe lattice: } \mathcal{A}(i\omega_n)=\frac{t_*^2}{2}G(i\omega_n)\ . \tag{9}$$

Due to the absence of loops in this case, the effective on-site amplitude just coincides with the on-site Green's function itself.

It is instructive to check these equations in two simple limits. In the free limit $U=0$, (5) is solved by $G^{-1}=i\omega_n+\mu-\mathcal{A}$, and hence from (6), $G(i\omega_n)=\tilde{D}(i\omega_n+\mu)$ reduces to the free on-site Green's function ($\Sigma=0$). In the "atomic" limit $t_*=0$, one just has a collection of disconnected sites and $D(\epsilon)$ becomes a δ function, with $\tilde{D}(\zeta)=1/\zeta$. Then (6) implies $\mathcal{A}(i\omega_n)=0$ and the effective action $\mathcal{S}$ becomes essentially local in time and describes a four-state Hamiltonian which yields

$$G(i\omega_n)_{\mathrm{at}}=(1-n/2)/(i\omega_n+\mu)+n/2(i\omega_n+\mu-U)\ ,$$

with

$$n/2=(e^{\beta\mu}+e^{\beta(2\mu-U)})/(1+2e^{\beta\mu}+e^{\beta(2\mu-U)})\ .$$

The above equations are valid in the absence of any spin or translational symmetry breaking. In the following, however, we shall need a generalization of these equations[4,7] to the following cases.

(i) Uniform applied field $h\sum_i(n_{i\uparrow}-n_{i\downarrow})$. The above equations are then trivially extended by separating the two spin species, allowing for two different amplitudes $\mathcal{A}_\uparrow,\mathcal{A}_\downarrow$ in $\mathcal{S}$, replacing $\mathcal{A}$ everywhere by the corresponding $\mathcal{A}_\sigma$ and μ by $\mu+h\sigma$. In particular, the self-consistency relation does not mix spin species, and reads

$$G_\sigma=\tilde{D}(\mathcal{A}_\sigma+G_\sigma^{-1})\ . \tag{10}$$

(ii) Antiferromagnetic phase with two-sublattice long-range order. Again, one has to allow for two separate amplitudes $\mathcal{A}_\uparrow,\mathcal{A}_\downarrow$ in $\mathcal{S}$, but the self-consistency condition now mixes both spin species, and reads (on, e.g., sublattice A)

$$G_\sigma=\sqrt{\zeta_{-\sigma}/\zeta_\sigma}\,\tilde{D}(\sqrt{\zeta_{-\sigma}\zeta_\sigma}) \tag{11}$$

with $\zeta_\sigma=\mathcal{A}+G_\sigma^{-1}=i\omega_n+\mu-\Sigma_\sigma$. The self-energy is still purely site diagonal, but depends on the sublattice, with $\Sigma_{A\uparrow}=\Sigma_{B\downarrow}$ ($\simeq\Sigma_\uparrow$) and $\Sigma_{B\uparrow}=\Sigma_{A\downarrow}$ ($\simeq\Sigma_\downarrow$).

One is also interested in computing *response functions* (e.g., spin and charge susceptibilities) of the lattice model. It is possible to reduce this calculation to a set of linear equations involving vertex functions of the *impurity problem*.[16,8] This has been successfully used in actual computations.[8] In the following, however, we use an alternative method, which is to solve the above equations for the *single-particle* Green's functions in the presence of a finite external "field" (e.g., h or μ), and to deduce the response function from the small field behavior. This method avoids the calculation of vertex functions and provides information on the finite-field behavior, which is of great physical interest in itself, especially for the response to a uniform magnetic field (Sec. V D).

Thermodynamic properties can also be obtained from impurity-model quantities. The single-particle Green's function directly yields the internal energy[17]

$$\frac{E}{N}=T\sum_{n,\sigma}\int_{-\infty}^{+\infty}d\epsilon\frac{\epsilon D(\epsilon)}{i\omega_n+\mu+h\sigma-\Sigma_\sigma(i\omega_n)-\epsilon}$$
$$+\tfrac{1}{2}T\sum_{n,\sigma}\Sigma_\sigma(i\omega_n)G_\sigma(i\omega_n) \tag{12}$$

while the grand-canonical free energy of the lattice model is related to the impurity model free energy by[7,4]

$$\frac{\Omega}{N}=\Omega_{\mathrm{imp}}-T\sum_{n,\sigma}e^{i\omega_n 0^+}\left[\int_{-\infty}^{+\infty}d\epsilon\,D(\epsilon)\ln[i\omega_n+\mu+h\sigma-\Sigma_\sigma(i\omega_n)-\epsilon]+\ln G_\sigma(i\omega_n)\right]\ . \tag{13}$$

This paper deals with the properties of the half-filled case, $\langle n_\uparrow\rangle+\langle n_\downarrow\rangle=1$. Then, particle-hole symmetry implies that $\mu=U/2$, and it is useful to define "shifted" quantities by

$$\hat{G}_0^{-1}\equiv G_0^{-1}-U/2,\quad \hat{\Sigma}\equiv\Sigma-U/2\ . \tag{14}$$

In addition to the standard fermionic symmetry, $G_\sigma(\tau+\beta)=-G_\sigma(\tau)$, the following symmetry properties then hold:

$$F_\sigma(-i\omega_n)=-F_{-\sigma}(i\omega_n)$$
$$\Longleftrightarrow F_\sigma(\beta-\tau)=-F_{-\sigma}(\tau)(\text{half filling})\ , \tag{15}$$

where F stands for any of the functions $G,\mathcal{A},\hat{\Sigma}$, and $\hat{G}_0$. In particular, note that

$$G_\sigma(\tau=0^-)=\langle n_\sigma\rangle=1-\langle n_{-\sigma}\rangle=1+G_\sigma(\tau=0^+)\ .$$

C. Connection with single-impurity models

As pointed out in Refs. 3 and 4, the single-site action (5) can be thought of as describing a magnetic impurity coupled to a bath of conduction electrons. In this picture, the single site plays the role of the impurity orbital, while the role of the bath is played by the rest of the lattice, which generates $\mathcal{A}(\tau-\tau')$. The hybridization is via the hopping t_*. This point of view can be made precise by introducing the following spectral representation:

$$\mathcal{A}(i\omega_n)=\int_{-\infty}^{+\infty}\frac{\Delta(\omega)}{i\omega_n-\omega}d\omega\ . \tag{16}$$

With this parametrization, the action $\mathcal{S}$ exactly coincides with the effective action for the d orbital in the Anderson model,[18] once all conduction electrons have been integrated out. To see this, let us consider the Anderson model (in the particle-hole symmetric case, corresponding to half-filling, for simplicity):

$$H_{\rm AM}=\sum_{k\sigma}\omega_k a_{k\sigma}^{\dagger}a_{k\sigma}+U(n_{d\uparrow}-\tfrac{1}{2})(n_{d\downarrow}-\tfrac{1}{2})+\sum_{k\sigma}[V_k a_{k\sigma}^{\dagger}d_{\sigma}+\text{H.c.}]\ . \tag{17}$$

Performing the Gaussian integral over the $a_{k\sigma}$'s, the effective action for the d level is found to coincide with $\mathcal{S}$ with the identifications $\mu=U/2$ and $\Delta(\omega)_{\rm AM}=\sum_k|V_k|^2\delta(\omega-\omega_k)$. Hence the spectral density $\Delta(\omega)$ associated with $\mathcal{A}(i\omega_n)$ can be thought of as the density of states defining the conduction electron "bath" in the Anderson model picture. This is even more clear in the case of the Bethe lattice: there, one can identify $V_k=t_*/\sqrt{2}$ as the effective hybridization and the self-consistency can be written as $\Delta(\omega)=(t_*/\sqrt{2})^2\rho(\omega)$, which means that the density of states of the bath coincides with the one-particle local spectral density $\rho(\omega)=-1/\pi\,\mathrm{Im}G(\omega+i0^+)$.

Equivalently, one could view the single-site action as a Wolff model [i.e., an electron gas with DOS $\rho(\omega)$ in which U acts only on a single site[19]].

III. METHODS OF SOLUTION

A calculation of the one-particle properties of the $d=\infty$ Hubbard model requires a solution of the *coupled* problem defined by Eqs. (5) and (6). The amplitude $\mathcal{A}(i\omega_n)$ (or alternatively, the "bare" Green's function of $\mathcal{S}$: $G_0(i\omega_n)\equiv[i\omega_n+\mu-\mathcal{A}(i\omega_n)]^{-1}$) is not explicitly known from the start. Hence, we use a method based on the iteration of the two following steps: (i) the calculation of the impurity Green's function G for a given G_0 (ii) the calculation of an updated function $G_{0,\rm new}$ from the above solution. This is achieved by first Fourier transforming[20] G_0 and G and then using the self-consistent equation (6) in the form

$$G_{0,\rm new}(i\omega_n)=\Sigma(i\omega_n)+1/\tilde{D}[i\omega_n+\mu-\Sigma(i\omega_n)]\ ,$$

where $\Sigma(i\omega_n)\equiv G_0(i\omega_n)^{-1}-G(i\omega_n)^{-1}$.

This procedure is iterated at a fixed value of the chemical potential μ until convergence is reached, starting from an arbitrary G_0.

The difficult step of this procedure is (i), which involves solving the impurity model $\mathcal{S}$ for an essentially arbitrary G_0.[21] This is a nonlinear problem, which is also nonlocal in time, and a full solution can only be numerical.[8–10] Alternatively, one can resort to approximations to make the problem tractable. In the next subsections, we describe two methods based on these two possible strategies.

A. Numerical solution: Monte Carlo and exact enumeration methods

Since $\mathcal{S}$ can be viewed as an Anderson model, we can use the algorithm of Hirsch and Fye[22] in order to perform step (i). This algorithm works directly in terms of the imaginary-time Green's functions $G_0(\tau)$ and $G(\tau)$. The interval $[0,\beta]$ is discretized in L slices of size $\Delta\tau$, $\tau_i=i\Delta\tau$, $i=0,\ldots,L-1$ ($\beta=L\Delta\tau$). After the usual Trotter breakup, the interaction term in $\mathcal{S}$ is decoupled through L auxiliary Ising variables $\sigma(\tau_i)$:

$$e^{-\Delta\tau U n_\uparrow n_\downarrow}=\tfrac{1}{2}\mathrm{Tr}\sigma e^{\lambda\sigma(\tau_i)(n_\uparrow-n_\downarrow)-U\Delta\tau(n_\uparrow+n_\downarrow)/2} \tag{18}$$

with $\cosh\lambda=\exp\Delta\tau U/2$. For a given spin configuration, the trace over fermions can be taken. The computation of $G(\tau_i)$ amounts to finding the inverse of the L^*L matrix

$$O(\tau_i,\tau_i')=\hat{G}_0^{-1}(\tau_i-\tau_i')+\lambda\sigma(\tau_i)\delta_{\tau_i,\tau_i'}$$

for each of the 2^L spin configurations and to summing over configurations with a statistical weight given by the determinant of the matrix O:[23] $G(\tau-\tau')=\langle O^{-1}(\tau,\tau')\rangle_{\text{spin conf}}$. Following Hirsch and Fye,[22] this can be done most conveniently by sampling the Ising configuration space through single spin flips, and making use of Dyson's equations instead of computing explicitly the inverse of O. This reduces the number of operations from L^3 to L^2 per accepted move.

For large grids ($L\geq 18$) we have used a single-spin-flip Monte Carlo method to sample spin configurations, as in Ref. 22. For $L\leq 16$, we have been able to sum over *all* 2^L spin configurations using Gray's code,[24] which enumerates all configurations through single spin flips. This enumeration method is free of statistical noise, and can thus be considered as an *exact numerical solution* of the problem for a given discretization. Even though it is limited in grid size L, it has several advantages over the Monte Carlo method.

(1) It allows a direct calculation of the energy and free energy, using Eqs. (12) and (13).

(2) It is better suited for analytic continuations of imaginary-time data using simple Pade transform methods (rather than maximal entropy ones) (Ref. 25).

(3) It allows a precise assessment of convergence properties.

Remarkably, this iterative algorithm is found to converge rapidly to a solution (G_0,G) of Eqs. (5) and (6). Typical examples are displayed in Fig. 1 for $U=2.5$ and 5 at $\beta=10$. The results displayed are obtained by the Monte Carlo method with $L=32$, for which a conver-

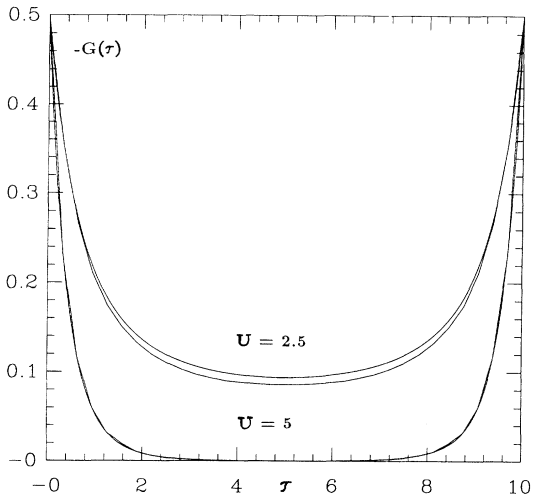

FIG. 1. The hypercubic lattice local Green's function $-G(\tau)$ vs τ at $\beta=10$, for $U/t_*=2.5$ (upper group of curves) and $U/t_*=5$ (lower group). Within each group, the lower curve is the Monte Carlo solution with $L=32$, and the upper one is the result of the iterated perturbation theory (IPT) approximate method.

gence up to 10^{-3} is obtained in four iterations with 10 000 sweeps. For the same number of iterations, an accuracy of 10^{-5} is reached when using Gray's code with $L=16$ (3 min per iteration on a HP 730 workstation).[26]

B. Iterated perturbation theory

Powerful as it is, the above numerical method is still limited by the two intrinsic weaknesses of the algorithm used: studying low temperatures requires a rapidly increasing numerical effort, and, more importantly, the algorithm produces imaginary-time quantities which do not directly yield the dynamical properties of the system (an analytic continuation is required). Hence, an approximate method which is able to deal directly with zero temperature and real frequencies is of interest. For the single-impurity problem, the interaction term $Un_\uparrow n_\downarrow$ is known to be a fairly regular perturbation, and much useful qualitative and quantitative information on the Anderson model has been obtained in the past using weak-coupling approaches.[27]

Motivated by this remark, a method was introduced in Ref. 3, which is again based on the iteration of steps (i) and (ii), but simply makes use of a weak-coupling calculation to second order in U in order to compute the self-energy Σ (and hence G) from G_0 in step (i). We call this method the iterated perturbation theory (IPT). Obviously, it can be easily performed at any finite temperature, or directly at zero temperature using real-frequency Green's functions

$$G(\omega)=\theta(\omega)G(\omega+i0^+)+\theta(-\omega)G(\omega-i0^+) .$$

The relevant formulas read (at half filling)

$$\hat{\Sigma}_\sigma(i\omega_n)=U^2\int_0^\beta d\tau\, e^{i\omega_n\tau}\hat{G}_{0,-\sigma}(\tau)^3 , \tag{19}$$

$$T=0:\ \hat{\Sigma}_\sigma(\omega)=-U^2\int_{-\infty}^{+\infty} dt\, e^{i\omega t}\hat{G}_{0,-\sigma}(t)^3 . \tag{20}$$

Various alternative methods based on weak-coupling have been used by other authors in the present context of the $d=\infty$ lattice model, namely, plain weak-coupling perturbation theory to $O(U^2)$ in which the *free* local Green's function $\tilde{D}(i\omega_n)$ is used in (19) and (20) in place of $\hat{G}_0$,[28] and self-consistent weak-coupling approaches[29] which attempt to find a solution with the *interacting* G replacing $\hat{G}_0$ in (19) and (20). This has also been generalized to include bubble and ladder summations in Ref. 30.

All three methods, of course, coincide for very small values of U. It has been noticed, however,[3] that the results of the self-consistent perturbation theory are in *qualitative disagreement* with both plain weak coupling and IPT already for moderate values of U: only the latter method accounts correctly for the high-energy properties of the excitation spectrum, and, in particular, for the formation of the upper Hubbard band.

Recently, insightful remarks by Zhang *et al.* have put the IPT method on a much firmer basis.[11] They noticed that, remarkably, IPT yields the *exact result* in the *atomic limit* $t_*=0$ at half filling. Indeed, the self-consistency equation (6) implies that $\hat{G}_0=1/i\omega_n$ in this limit, for which formulas (19) and (20) lead to $\hat{\Sigma}=U^2/4i\omega_n$, the exact atomic answer. From this remark, one can expect IPT to provide a satisfactory *interpolation between the small- and large-U limits.* Indeed, as first noticed in Ref. 11, a coupled solution of the IPT equations can be found at *arbitrary large values of U* and is found to be in remarkable agreement with the corresponding numerical results down to the lowest temperatures where the latter can be obtained. A direct comparison is made in Fig. 1 for $U=2.5$ and 5 at $\beta=10$. It will be shown below that the paramagnetic solution has a phase transition for a finite $U=U_c$ at $T=0$, which is quite correctly described within IPT, a feature obviously not found within a plain weak-coupling expansion.

IV. PHASE DIAGRAM AND PHASE TRANSITIONS

To make the reading of this paper easier, we give at this stage an overview of the phase diagram found at half filling using the above methods. Figure 2 displays the phase diagram for the hypercubic lattice as a function of temperature T and strength of the interaction U. Very similar results are found for the Bethe lattice. The *equilibrium* phases of the Hubbard model on both lattices are the following.

(i) An antiferromagnetic (AF) phase for $T<T_N(U)$. This phase is found by solving the mean-field equations taking into account two-sublattice long-range order, as described above. Iteration of these equations is found to converge to a broken symmetry solution with a nonzero staggered magnetization m_s for $T<T_N$, and to an unbroken solution above T_N. That the ground state is always antiferromagnetic for arbitrary U is to be expected from the bipartite character of both lattices [with $D(0)>0$].

(ii) A paramagnetic phase for $T>T_N(U)$. Another critical line $U=U_c(T)$ is indicated in Fig. 2, which corresponds to a phase transition found within the IPT

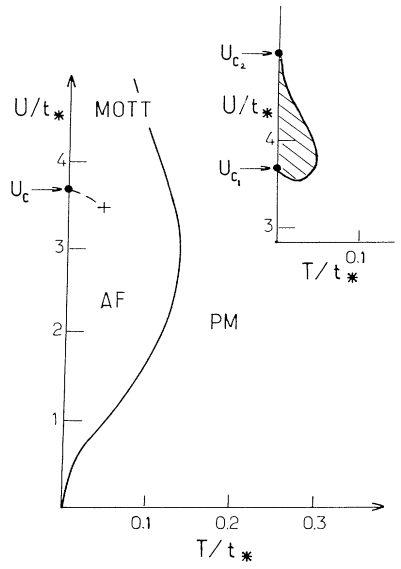

FIG. 2. Phase diagram for the hypercubic lattice. The plain line is the Néel temperature below which the antiferromagnetic (AF) phase is found. Within the IPT method, a (dashed) line of first-order transition is found between a paramagnetic metal (PM) and a Mott paramagnetic insulator (MOTT). Inset: Region of *coexistence* of a metallic and an insulating solution of the mean-field equations, as obtained in the IPT method (see also Ref. 11).

method when solving the paramagnetic form (5) and (6) of the mean-field equations, ignoring the possibility of spin-symmetry breaking. This instability has been reported previously,[9,10] and corresponds, at zero temperature, to a Mott-Hubbard transition between a paramagnetic metal for $U<U_c(T=0)\equiv U_c$ and a paramagnetic insulator for $U>U_c$. Our work and the complementary results of Ref. 11 show that $U=U_c(T)$ is a line of first-order transition (similar to a liquid-gas situation) which ends at a critical point. More precisely, we find that, close to $T=0$, an insulating solution of the paramagnetic mean-field equations can be found for $U>U_{c1}$ while, as recently reported in Ref. 11, a metallic solution exists in the whole range $U<U_{c2}$, with $U_{c2}>U_{c1}$. Hence, there is a region of the (U,T) parameter space in which *two solutions* of the equations coexist, and one has the characteristic scenario of a first-order transition. Using the IPT approximate scheme, one finds $U_c/t_*\simeq U_{c1}/t_*\simeq 3.7$ on the hc lattice ($\simeq 3.6$ on the Bethe lattice), and[11] $U_{c2}/t_*\simeq 4.5$ ($\simeq 4.7$ on the Bethe lattice). The coexistence region found within IPT is displayed in the inset of Fig. 2. Note that it extends only up to temperatures of order $\simeq\frac{1}{20}$. For the true (Monte Carlo) solution, the situation is somewhat unclear and deserves further numerical calculations. The nature of the Mott transition is discussed more extensively in Sec. VI E.

Let us emphasize that the metal-insulator transition at $T=0$ is not a transition occurring within the true ground state of the model (which is an antiferromagnetic insulator for all U), but only within the paramagnetic solution continued to the region where it is actually unstable towards antiferromagnetism. That such a continuation is possible (in a fully consistent way thermodynamically) will be demonstrated at length below, and is a remarkable feature of the $d=\infty$ mean-field equations. In fact, an alternative model can be found for which the paramagnetic Mott-Hubbard state is the exact ground state, without any magnetic order setting in at low temperatures.[31] It is simply defined as a Hubbard model on a *fully connected* cluster of N sites, with randomness on the hopping parameters t_{ij}:

$$H=-\sum_{\sigma;i,j=1}^{N} t_{ij}c_{i\sigma}^{\dagger}c_{j\sigma}+U\sum_i n_{i\uparrow}n_{i\downarrow}\quad \sqrt{\overline{t_{ij}^2}}=\frac{t_*}{\sqrt{2N}}\ . \tag{21}$$

It is possible to show[31] that, *in the paramagnetic phase,* the single-particle Green's function of this random model coincides with the same quantity for the Hubbard model on the $z=\infty$ Bethe lattice, with no randomness and hopping parameter $t_{ij}=t_*/\sqrt{2z}$.[32] It is clear, however, that the phase diagram of the two models differ: obviously the disordered one has a highly degenerate total singlet ground state for large U at half filling, and *no antiferromagnetic phase.* Hence, a true ground-state phase transition is found for this model between a paramagnetic Mott insulator at large U and a metal at small U. The rest of this paper is devoted to a detailed discussion of the physical properties of these various phases.

V. THE PARAMAGNETIC ITINERANT REGIME

We discuss here the physics of the paramagnetic phase below the Mott-Hubbard transition. We consider, when needed, the continuation of the paramagnetic solution down to $T=0$, ignoring in this section the occurrence of antiferromagnetism (which will be addressed in Sec. VII).

A. Energy scales and thermodynamic properties

We have computed several thermodynamic quantities as a function of temperature and U, both using the exact enumeration numerical solution and the IPT scheme at finite temperature. The basic quantity computed is the internal energy, which can be readily obtained from the imaginary-time Green's function using Eq. (12). The specific heat $C_v=d(E/N)/dT$ is then obtained by performing the simulation for two close temperatures and differentiating numerically.[33] The same calculation allows one to obtain the entropy by integration:

$$\frac{S}{N}=\ln(4)-\int_T^{+\infty}\frac{C_v(T')}{T'}dT'\ , \tag{22}$$

where we have used the high-temperature limit of ln4 (corresponding to the four possible states on each site). Note that Eq. (22) only requires knowing C_v *above* the temperature studied. Another possibility would be to compute directly the free energy from Eq. (13) but we have preferred the more economical method described here which requires only the knowledge of Green's functions.

In Fig. 3, the results obtained for C_v vs T by the

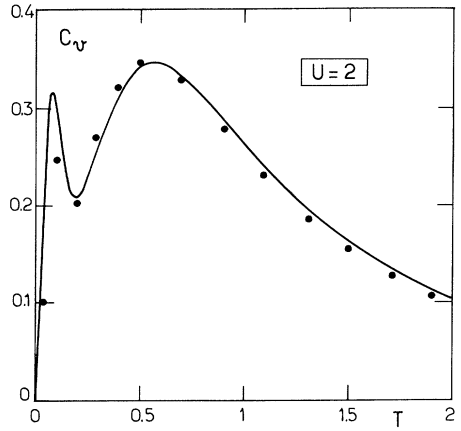

FIG. 3. Specific heat C_v vs temperature T for $U=2$ (hypercubic lattice). The points are the results of the numerical solution using exact enumeration, extrapolated to $\Delta\tau\to 0$. The solid line is obtained by the IPT method. Note that the spin and charge energy scales are already well separated.

enumeration method and the IPT scheme are displayed and compared for $U=2$. The agreement is seen to be spectacular, down to the lower temperatures studied by enumeration. This confirms for thermodynamic quantities the observation made in Ref. 11 for Green's functions. Figure 4 displays the C_v vs T curves for several values of $U<U_c$, ranging from the weak-coupling regime to the very strongly correlated metal for U close to U_c. Increasing U leads to the formation of two peaks in the specific heat, corresponding to the gradual separation of two energy scales.

(i) A low-energy scale T_F^* (or effective Fermi temperature), corresponding to the first, narrow peak in C_v vs T. As discussed below, T_F^* must be interpreted as a scale associated with local spin fluctuations and is also the scale below which a Fermi-liquid description applies. In particular, the specific heat starts linearly at low temperature, and a possible definition of T_F^* is from its slope: $C_v=T/T_F^*$ as $T\to 0$. This yields, e.g., $T_F^*(U=0)=3/2\pi^2 D(0)\simeq 0.27$ and $T_F^*(U=2)\simeq 0.13$ (hypercubic lattice). T_F^* sets the scale for both the location and the width of the specific-heat peak (with this definition, T_F^* is found to lie roughly halfway between the peak maximum and the subsequent minimum). As U is increased, T_F^* decreases rapidly. The ratio $T_F^*(U)/T_F^*(0)$ is related to the effective mass and quasiparticle weight Z by (cf. Sec. V B and Fig. 8, where a plot of this ratio is given)

$$\frac{T_F^*(U)}{T_F^*(0)}=\frac{m}{m^*}=Z\ . \tag{23}$$

(ii) A high-energy scale (set by U), corresponding to the broad high-energy peak in C_v vs T. This scale is associated with on-site charge fluctuations. As U is increased, the location of this peak shifts upwards, but its width remains roughly constant, set by the bare bandwidth.

Interestingly, an intermediate range of U is found in which C_v vs T does not yet have two well-separated peaks, but rather displays a plateaulike feature (or a very shallow minimum) around T_F^*. This regime is somewhat reminiscent of the properties of liquid ^{3}He (Ref. 34) (though C_v eventually decreases in our present model because of the bounded DOS). Another puzzling feature of the results displayed in Fig. 4 is that all curves appear to cross almost at the same temperature, i.e., there apparently is a special temperature ($\simeq 0.6t_*$ for the hc lattice) at which the specific heat is independent of the strength of the interaction, to quite good accuracy. We have no simple physical explanation of this phenomena, but we note that a very similar phenomenon occurs in liquid ^{3}He,[34] if one views U as playing the role of pressure as in the quasilocalized approach.[36,35] As shown below (Fig. 15), this single crossing no longer holds in the insulating phase above U_c.

A typical result for the entropy per lattice site vs temperature is displayed in Fig. 5, for $U=2$. The overall behavior is much smoother than for C_v, but the different regimes, corresponding to the two energy scales above,

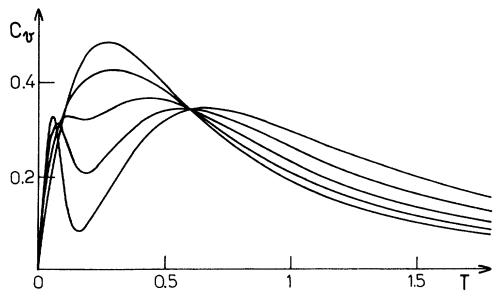

FIG. 4. Specific heat vs temperature (hc lattice) for $U=0.51$, 1, 1.5, 2, 2.5. Note the gradual increase of the linear slope with U and the gradual separation of the spin and charge scales. The curves seem to intersect at essentially the same temperature.

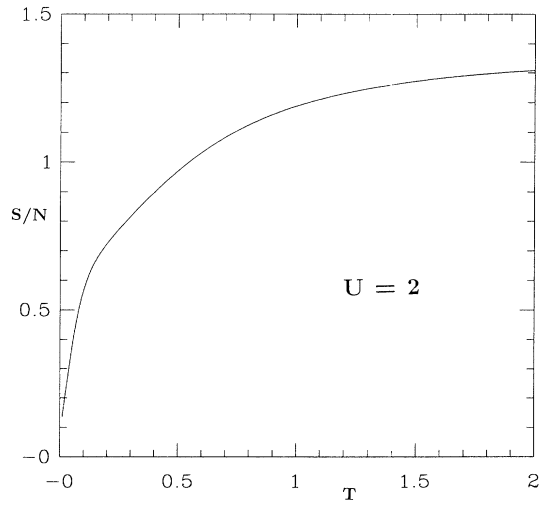

FIG. 5. Entropy per lattice site S/N vs temperature for $U=2$ (hc lattice). The value ln2 is reached roughly at the spin fluctuation scale T_F^*.

are quite clearly seen. S/N starts linearly at low temperatures, and, interestingly, reaches a value close to ln2 around $T \simeq T_F^*$. This corresponds to the defreezing of the on-site spin fluctuation entropy at this scale, and is also qualitatively similar to the experimental results on ^{3}He.[34] A second regime of temperature between T_F^* and $\simeq U$ corresponds to the progressive defreezing of charge fluctuations, with a slow increase of S/N from ln2 to ln4.

As a simple thermodynamic indicator of the degree of correlation of the system, we display in Fig. 6 the temperature dependence of the fraction of doubly occupied sites: $\langle D \rangle = \langle n_\uparrow n_\downarrow \rangle$, for various values of U. This is easily computed as an average over Ising spin configurations in the numerical simulation of the single-site problem (note that $\langle D \rangle$ is related to the impurity orbital local moment by $2\langle D \rangle = 1 - \langle S_z^2 \rangle$). At very high temperature ($T \gg U$), $\langle D \rangle$ becomes asymptotic to the atomic value $\langle D \rangle_{\text{at}} = 1/[2+2\exp(U/2T)]$ and tends to $\frac{1}{4}$ as expected. The data display a characteristic low-temperature behavior: for U not too large, $\langle D \rangle$ initially *decreases* with temperature, reaches a minimum for $T = T_m$, and increases again. The inset of Fig. 6 shows the dependence of T_m on U. This behavior is characteristic of incipient localization effects in a strongly correlated Fermi liquid in a regime dominated by spin fluctuations.[37] Starting from the low-temperature Fermi-liquid regime with an entropy $\simeq T/T_F^*$ per particle, the system can gain free energy when increasing temperature by increasingly localizing the particles (i.e., decreasing $\langle D \rangle$) in order to take advantage of a larger spin entropy. The same physical reason is responsible for the negative slope of the metal-insulator transition line $U_c(T)$ (Fig. 2), so that one can go from the itinerant to the localized phase upon heating. This is also observed in the phase diagram of liquid ^{3}He below the Pomeranchuk temperature and of transition-metal oxides such as V_2O_3.[38]

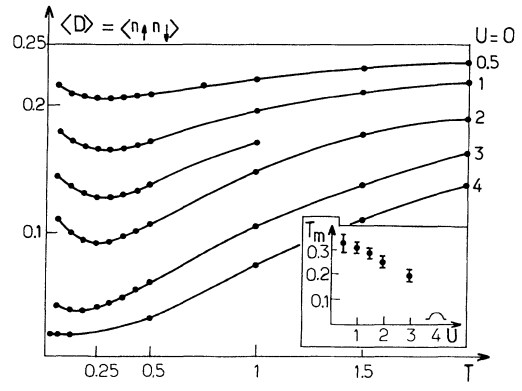

FIG. 6. Fraction of doubly occupied sites $\langle D \rangle$ vs temperature for the hc lattice with $U=0$, 0.5, 1, 2, 3, 4 (exact enumeration and Monte Carlo results). Inset: Temperature T_m at which the minimum of $\langle D \rangle$ vs T is found, as a function of U. For $U=4$, we cannot find a minimum down to the lowest temperature studied ($\beta=32$).

B. Zero-temperature results and Fermi-liquid description

We now study, using the IPT method, the zero-temperature properties of the metallic solution of the paramagnetic equations, which exists[11] for $U < U_{c2}$. Typical results for the real and imaginary parts of the $T=0$ (retarded) self-energy are displayed in Fig. 7. A Fermi-liquid description of the low-frequency behavior applies, with

$$\mathrm{Re}\Sigma(\omega+i0^+) = U/2 + (1-1/Z)\omega + O(\omega^3) , \quad (24)$$

$$\mathrm{Im}\Sigma(\omega+i0^+) = -\gamma\omega^2 + O(\omega^4) . \quad (25)$$

The constant term $U/2$ is such that the Luttinger theorem is satisfied, with $\Sigma(i0^+) = \mu = U/2$, so that the Fermi surface is unchanged by the interactions in the metallic phase. Note that, because $\Sigma(\omega)$ is momentum independent, the Fermi surface not only retains its volume, but also its *shape*.[13] For the same reason, the quasiparticle weight Z is directly related to the effective mass by[13] $m^*/m = 1/Z$ and controls the spin-fluctuation scale introduced above [Eq. (23)]. A plot of the IPT results for Z is given in Fig. 8 for both the hypercubic and Bethe lattices. Z decreases rapidly with increasing U, and jumps discontinuously to zero at the first-order Mott transition $U_c(T=0)$ (the values of Z corresponding to the metallic solution in the range $U_c < U < U_{c2}$ are not displayed in Fig. 8). We also display in Fig. 9 the momentum distribution of particles $N(\epsilon_k)$, showing the progressive reduction of the discontinuity (of height Z) as U is increased.

The IPT method also yields information about the excitation spectrum, through the $T=0$ local one-particle spectral density:

$$\rho(\omega) = -\frac{1}{\pi}\mathrm{Im}\sum_{\mathbf{k}} G(\mathbf{k},\omega+i0^+) . \quad (26)$$

This quantity is displayed in Fig. 10 for several values of U. As U is increased from zero, $\rho(\omega)$ develops three well-separated structures:[3] a narrow quasiparticle peak

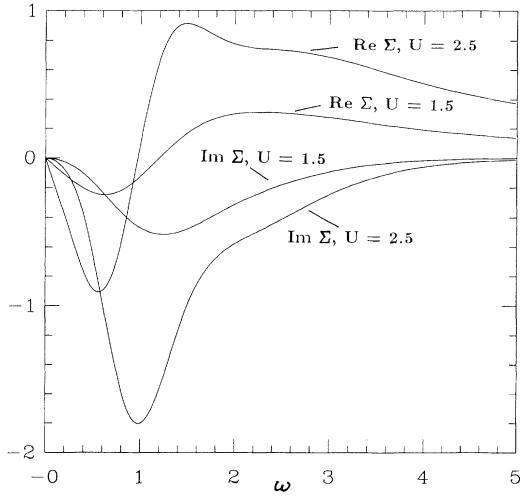

FIG. 7. $\mathrm{Re}\Sigma(\omega+i0^+)$ and $\mathrm{Im}\Sigma(\omega+i0^+)$ at $U=1.5$ and 2.5 (hc lattice, IPT method).

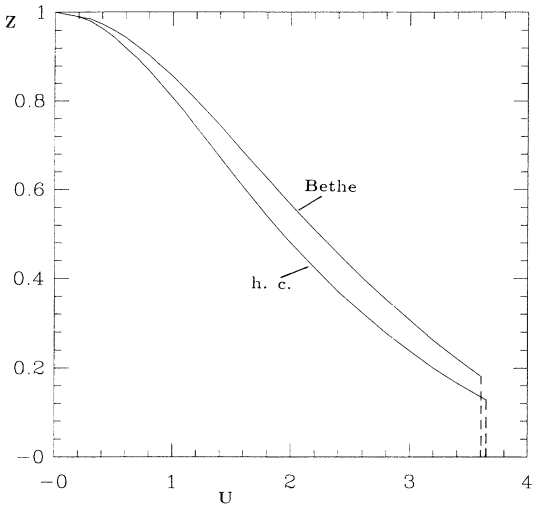

FIG. 8. Quasiparticle weight Z as a function of U for the hc lattice (lower curve) and Bethe lattice (upper curve), as obtained by IPT. Z directly yields the effective mass and spin-fluctuations scale (Kondo temperature) from $Z=m/m^*=T_F^*(U)/T_F^*(0)$. Note that the Gutzwiller approximation yields the straight line $Z_{GA}=1-U/U_{BR}$, with $U_{BR}=8\epsilon_0\simeq 4.5$ for the hc lattice ($\simeq 4.8$ for the Bethe lattice).

centered at $\omega=0$, and broad high-energy satellite peaks on a scale set by U. This parallels the above results for C_v.

As a consequence of the Luttinger theorem, the height of the quasiparticle peak remains equal to its free value independently of the interaction strength U.[13] Its width is set by the quasiparticle weight Z and is thus proportional to T_F^* (for the hc lattice, the width at half-height can be estimated as $\simeq 2\sqrt{\ln 2}Zt_*\simeq 1.66Zt_*\simeq 6T_F^*$). Note the following low-frequency expansion of $\rho(\omega)$ obtained by inserting (24) and (25) into (26):

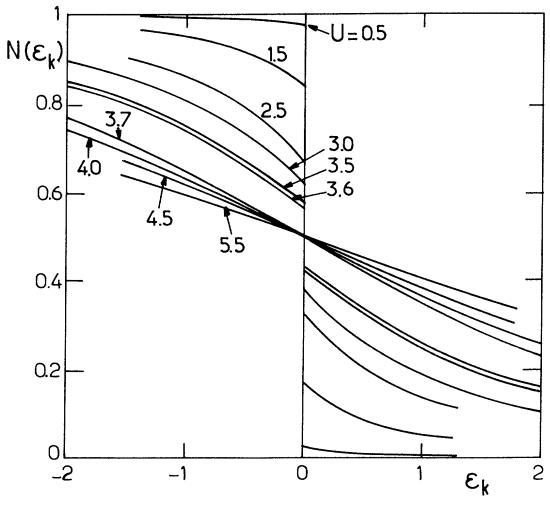

FIG. 9. Distribution of occupied states $N(\epsilon_k)$, for various values of U (hc lattice) within IPT. Note the absence of a jump for $U>U_c$ and the abrupt change of behavior above $U=3.6$.

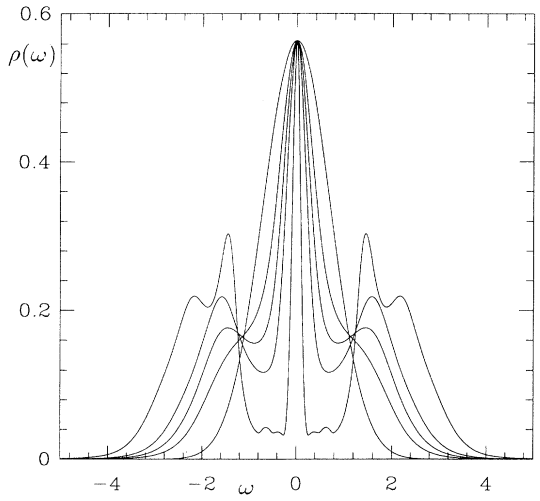

FIG. 10. IPT results for the local $T=0$ spectral density of the paramagnetic solution, $\rho(\omega)$ at $U=0$, 1.5, 2, 2.5, 3.65 (hc lattice).

$$\rho(\omega)=D(0)-\frac{1}{2}\omega^2\left[\frac{D_2}{Z^2}+\frac{2D_1\gamma}{\pi}\right]+O(\omega^4)\ , \qquad (27)$$

where $D_2=-D''(0)>0$ and $D_1=-\int d\epsilon\, D'(\epsilon)/\epsilon>0$ [$D(0)=1/\sqrt{\pi}$, $D_1=2$, $D_2=2/\sqrt{\pi}$ for the Gaussian DOS with $t_*=1$]. This shows that Z controls the curvature of the quasiparticle peak near $\omega=0$.

The satellite peaks can be interpreted as high-energy charge excitations signaling the formation of the upper Hubbard band. They are found to form already for moderate values of U,[3] both within the IPT scheme and when an analytic continuation is made on the exact enumeration results. This is in qualitative agreement with the results of straight $O(U^2)$ weak-coupling expansions,[28] but *not* with the self-consistent schemes of Refs. 29 and 30. The latter fail to reproduce the high-energy excitations correctly. Note that, for U large enough, we find that the upper Hubbard band acquires a two-peak structure. As discussed below, the lowest-frequency one can be viewed in a sense as a mirror image of the quasiparticle peak.

Let us mention that the overall shape of the spectral density and its dependence on U found here is in good qualitative agreement with recent photoemission experiments of several transition-metal oxides.[41]

Finally, we describe how the spectral density behaves for *finite* temperature. Figure 11 (a) illustrates the evolution of $\rho(\omega)$ when raising the temperature from $T=0$, with $U=3<U_c$. At a low-temperature scale given roughly by the half-width of ρ at $T=0$ (i.e., $\simeq 3T_F^*$), the quasiparticle peak is suppressed and the curvature of $\rho(\omega)$ near $\omega=0$ becomes negative. For completeness, we also display in Fig. 11(b) IPT results for $\rho(\omega)$ at a *fixed* temperature $\beta=7.2$, for increasing values of U. The same behavior is apparent. The curves in Fig. 11(b) agree very well with the results of Jarrell and Pruschke in Ref. 8 obtained by a maximal entropy continuation of Monte

Carlo data for the same parameters. This agreement gives us confidence in the accuracy of the IPT scheme.

C. Impurity-model interpretation: Local Kondo effect

The above properties have a simple interpretation[3] when following the analogy with a single-impurity Anderson model in the particle-hole symmetric case, described in Sec. II C. The important quantity to think about in this framework is the density of states of the effective conduction electron bath, $\Delta(\omega)$. Let us emphasize that, unlike the situation usually considered when discussing the one-impurity Anderson model, $\Delta(\omega)$ itself changes continuously with U here, and has strong frequency dependence as well. In the metallic phase, $\Delta(\omega=0)$ *remains finite* (and *independent of U*), while the width of $\Delta(\omega)$ around $\omega=0$ *decreases as U increases.*

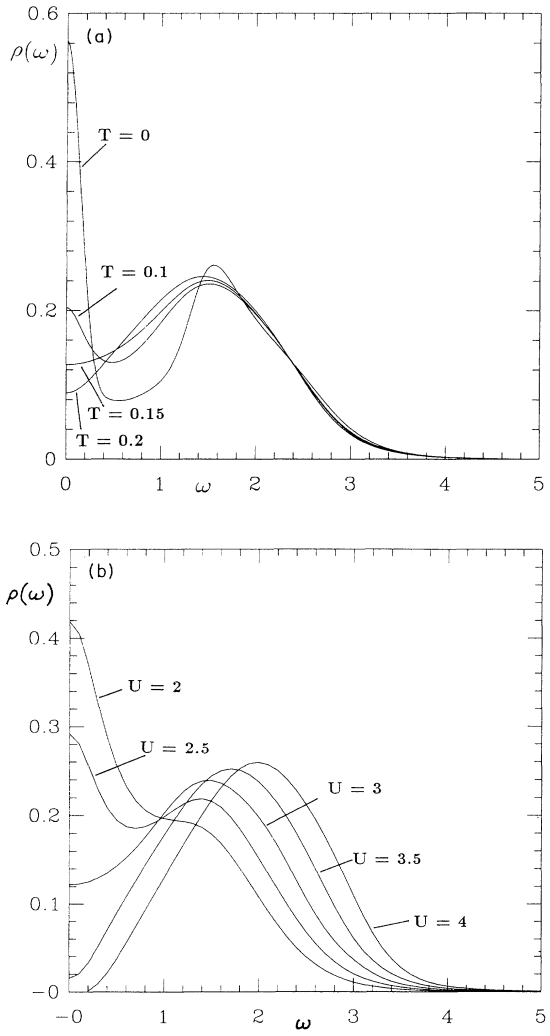

FIG. 11. (a) Local spectral density $\rho(\omega)$ at $U=3$ (hc lattice) for temperatures $T=0$, 0.1, 0.15, 0.2 (IPT method). The quasiparticle peak disappears at a scale set by T_F^*. (b) Local spectral density $\rho(\omega)$ at *finite temperature* $\beta=7.2$, for $U=2$, 2.5, 3, 3.5, 4 (IPT method). Very similar results were obtained in Ref. 8 using an analytic continuation of Monte Carlo data.

This is obvious for the Bethe lattice, for which $\Delta(\omega)=(t_*/\sqrt{2})^2\rho(\omega)$. More generally, it is apparent on the low-frequency expansion of $\Delta(\omega)$ obtained by making use of (24) and (25) into the self-consistency equation (6):

$$\Delta(\omega)=\Delta(0)+\Delta''(0)\omega^2/2+O(\omega^4)\ ,$$

with

$$\begin{aligned}\pi\Delta(0)&=\frac{1}{\pi D(0)}\ ,\\ \pi\Delta''(0)&=\frac{1}{[\pi D(0)Z]^2}\left[\pi D_2-\frac{2D_1^2}{\pi D(0)}\right]\\ &\quad+2\gamma\left[\frac{D_1}{[\pi D(0)]^2}-1\right]\ (<0)\ .\end{aligned}\tag{28}$$

Since $\Delta(\omega)$ is nonzero around $\omega=0$, one has the familiar situation of a magnetic impurity in a metal. The single-site problem enters a Kondo regime upon increasing U, with almost frozen charge fluctuations and on-site spin fluctuations between the two states $|\uparrow\rangle$, $|\downarrow\rangle$. In this framework, the low-temperature scale T_F^* $[=Z3\Delta(0)/2]$ must be interpreted as the Kondo temperature below which these spin fluctuations are quenched by the Kondo effect. As emphasized by Langreth[39] and Nozieres,[40] the properties of the impurity model below T_F^* are those of a local Fermi liquid described above. The quasiparticle peak in $\rho(\omega)$ may be interpreted in this framework as the Abrikosov-Suhl resonance. As a first crude approximation, the broad satellite peaks associated with the upper Hubbard band can be thought of as a superposition with equal weight $\frac{1}{2}$ of the two magnetic Hartree-Fock solutions. Hence, the nontrivial frequency dependence of the upper Hubbard bands reflects the strong frequency dependence of $\Delta(\omega)$. In particular, the additional peak appearing close to U_c can be viewed as a mirror image of the quasiparticle peak within the upper Hubbard band (note that it disappears in the insulator, cf. Fig. 13). In a renormalization-group picture, the metallic phase corresponds to a flow towards small U (or large hopping t_*), i.e., to the usual scaling towards strong Kondo coupling.

D. Response to a uniform field: Absence of metamagnetism

To complete the discussion of the physical properties of the Fermi-liquid phase, we report some results on the response of this phase to a uniform magnetic field. This is motivated in particular by remarkable recent experiments on liquid ^{3}He,[42] which indicate a smooth saturation of the magnetization as a function of field, with a magnetic susceptibility *decreasing* with increasing field. In contrast, the Gutzwiller approximation predicts a strong metamagnetic behavior of the Fermi liquid close to U_c, with a susceptibility which *increases* with field and a finite critical field above which the system is fully polarized ($m=1$).[36,37] Accordingly, a Maxwell relation suggests that consistent finite-temperature generalizations of the Gutzwiller approximation should lead to a susceptibility *increasing* with temperature at low temperature.[37]

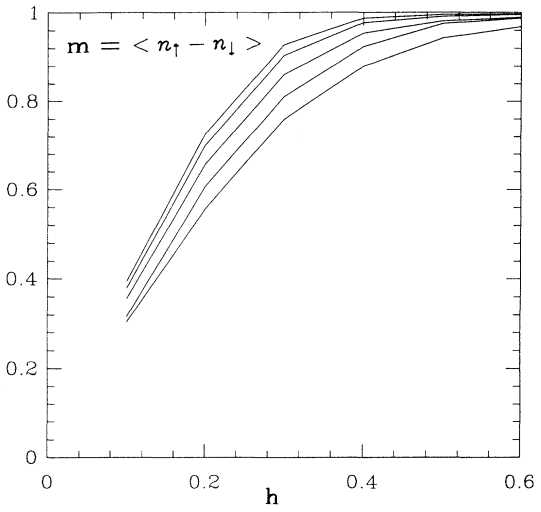

FIG. 12. Magnetization $m=\langle n_\uparrow - n_\downarrow \rangle$ vs applied uniform magnetic field h. From top to bottom: ($\beta=16$, $U=4$), ($\beta=16$, $U=3.5$), ($\beta=16$, $U=3$), ($\beta=8$, $U=3$), ($\beta=8$, $U=2.5$).

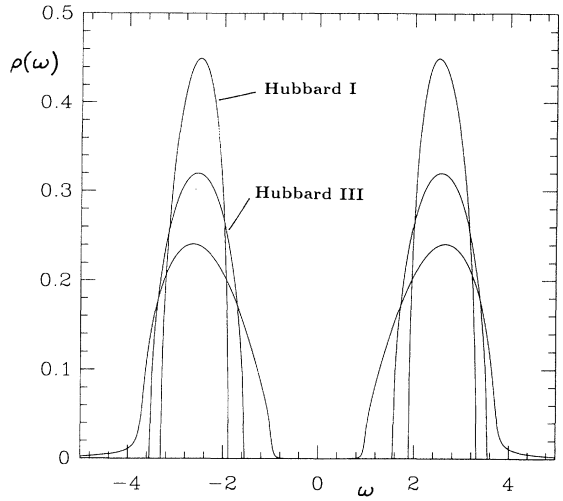

FIG. 13. Comparison of the IPT result for the $T=0$ local spectral density at $U=5$ (Bethe lattice) with the Hubbard I and Hubbard III approximations.

As explained above [Eq. (10)], the present method of solution is easily generalized to a uniform magnetic field h. Results obtained by exact enumeration with $L=16$ for the magnetization $m\equiv\langle n_\uparrow - n_\downarrow \rangle$ vs applied field, are displayed in Fig. 12 for $\beta=8$, $U=2.5$, 3 and $\beta=16$, $U=3$, 3.5, 4 (hc lattice). These results do not show any tendency to metamagnetic behavior. The magnetization smoothly saturates with field, and the susceptibility decreases upon increase of h. Comparison of the results for $U=3$ and $\beta=8$, 16 show that the susceptibility *decreases* with temperature. We also notice that, in contrast to the Gutzwiller approximation, the uniform susceptibility does not diverge as one crosses the metal-insulator transition (cf. Ref. 8).

These results show that the response to a uniform field is very poorly described by the Gutzwiller approximation. The underlying physical reason is that this approximation completely neglects charge fluctuations and residual magnetic exchange, which are of crucial importance for the magnetic properties of the true system.

VI. THE MOTT-HUBBARD LOCALIZED PHASE

A. Zero-temperature properties

Let us turn to the description of the insulating solution at zero temperature, found within the paramagnetic phase for $U>U_{c1}$. A typical IPT result for $\rho(\omega)$ in this phase is displayed in Fig. 13. The spectrum is purely incoherent, with no quasiparticle peak ($Z=0$). The upper Hubbard bands are not found to display any remarkable structure in the insulator, in contrast to the vicinity of the transition on the metallic side. For the Bethe lattice, one has a finite Mott-Hubbard gap Δ_g. For the hypercubic lattice, only a pseudogap is found, with $\rho(\omega)$ vanishing as $\omega\to 0$, but finite for all nonzero frequency. This is expected from the existence of tails extending from $-\infty$ to $+\infty$ in the $U=0$ Gaussian DOS: arbitrarily low-energy excitations (with very small weight) must always exist in that case. They correspond to the exponentially small fraction of electrons which live in the tails of the DOS and have an arbitrarily large (negative) kinetic energy. A simple argument suggests that $\rho(\omega)$ vanishes as e^{-1/ω^2} for small ω in this case. Note, however, that, despite this peculiarity, there is a clear sense in which a Mott transition arises also for the hypercubic lattice.

The self-energy itself has a markedly different behavior from the Fermi-liquid one. Let us concentrate for simplicity on the Bethe lattice for which the self-consistency equation (9) implies $\Sigma(\omega+i0^+)=\omega-t_*^2 G/2-1/G$. It follows from this equation that $\Sigma(\omega+i0^+)$ must be real inside the gap [since there $\rho(\omega)=-1/\pi\,\mathrm{Im}G=0$], except for a δ-function piece in $\mathrm{Im}\Sigma$ at $\omega=0$:

$$\mathrm{Im}\Sigma(\omega+i0^+)=0 \quad \text{for } \omega\in[-\Delta_g/2,\Delta_g/2],\quad \omega\neq 0 \tag{29}$$

and that $\mathrm{Re}\Sigma$ has the following low-frequency behavior:

$$\mathrm{Re}\Sigma(\omega+i0^+)=\frac{1}{\omega}\left[\int_{-\infty}^{+\infty} d\epsilon\frac{\rho(\epsilon)}{\epsilon^2}\right]^{-1}+O(\omega)\ . \tag{30}$$

A typical IPT result for $\mathrm{Re}\Sigma$, $\mathrm{Im}\Sigma$ is displayed in Fig. 14 for the Bethe lattice with $U=5$.

B. Comparison with Hubbard I and III approximations

It is of interest to compare the actual results for the spectral density to the predictions of the first approximate treatments included in Hubbard's original papers.

The simplest and crudest approximations (known as Hubbard I) amounts to replacing the self-energy with its atomic limit in the Green's function:[12]

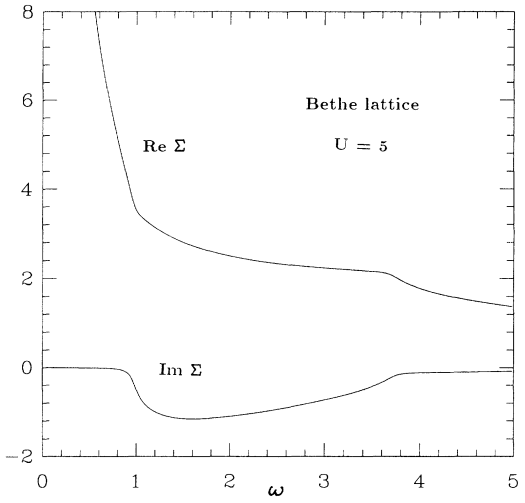

FIG. 14. $\mathrm{Re}\Sigma(\omega+i0^+)$ and $\mathrm{Im}\Sigma(\omega+i0^+)$ in the Mott-Hubbard phase at $U=5$ (Bethe lattice).

$$\text{Hubbard I: } G(\mathbf{k},i\omega_n)=\frac{1}{i\omega_n-\epsilon_k-U^2/4i\omega_n}\ ,$$

$$\text{i.e., } \rho(\omega)=D\left[\omega-\frac{U^2}{4\omega}\right]\ . \quad (31)$$

This expression incorrectly predicts an insulating solution with a gap for arbitrarily small values of $U>0$. It is compared to the actual $\rho(\omega)$ in Fig. 13 for $U=5$.

A more refined approximation is known as Hubbard III.[43] As recently emphasized in Ref. 10, it is easily understood on the mean-field equations (5) and (6). It amounts to solving in an approximate manner the single-site action (5), thinking of G_0^{-1} as an *almost local function of time*. Hence, the interacting Green's function of $\mathcal{S}$ is approximated by

$$G(i\omega_n)\simeq\frac{1}{2}\left[\frac{1}{\hat{G}_0(i\omega_n)^{-1}-U/2}+\frac{1}{\hat{G}_0(i\omega_n)^{-1}+U/2}\right]\ . \quad (32)$$

This is then used in the self-consistency condition (6) to get a closed equation for G, which reads

Hubbard III:

$$G(i\omega_n)=\tilde{D}\left[i\omega_n-\frac{1}{2G}[\sqrt{1+U^2G^2}-1]\right]\ . \quad (33)$$

For the Bethe lattice, this equation can be simplified into[10]

Hubbard III (Bethe lattice):

$$\tfrac{1}{4}G^3-\omega G^2+\left[\omega^2+\frac{2-U^2}{4}\right]G-\omega=0\ . \quad (34)$$

This equation does lead to a metal-insulator transition at $U_c^{\mathrm{III}}=\sqrt{2}t_*$. The corresponding $\rho(\omega)$ is also displayed in Fig. 13. Qualitatively, this approximation describes correctly the insulating regime, as recently emphasized in Ref. 10. Indeed, for very large U/t_*, G_0^{-1} does become local and the Hubbard III approximation provides a quick way to show that the paramagnetic solution must be insulating for large U. It fails completely on the metallic side, however, since it neglects all coherence effects. Quantitatively, it is clear from Fig. 13 that both the Hubbard I and Hubbard III approximations are quite inaccurate.

C. Thermodynamic and magnetic properties: Physical nature of the localized phase

Figure 15 displays specific-heat curves for the paramagnetic solution in the localized regime with increasing values of U (Bethe lattice). They have the expected activated behavior $\sim e^{-\Delta_g/T}$ at low temperature, and a broad maximum at high temperature associated with charge fluctuations involving the upper Hubbard band.

The entropy can also be obtained using Eq. (22), and is displayed in Fig. 16 for $U=5$. Remarkably, a residual entropy is found at zero temperature, with $S(T=0)$ very close to the value $N\ln 2$. This would be easy to understand in an oversimplified description of the localized phase, pictured as a collection of independent magnetic moments, as, e.g., in the Gutzwiller approximation. In the present context, however, it is surprising at first sight since the $d\to\infty$ limit does not neglect charge fluctuations and residual magnetic exchange. One must realize, however, that there are actually *two different exchange scales* in this limit: one is the exchange coupling between two fixed spins $J_{ij}\sim t_{ij}^2/U\sim O(1/d)$ while the other is the exchange energy between a spin and its shell of d antiparallel neighbors. Since the latter is d times the former, it remains $O(1)$ and sets the scale for the Néel temperature. The first scale does vanish as $d\to\infty$, and controls the splitting between singlet states with total $S_z=0$. Hence, the $d\to\infty$ limit *does lead to a degenerate ground state* if one insists on singlet states without long-range magnetic order, as discussed here.[44] This is especially clear for the fully connected random model mentioned in Sec. IV [Eq. (21)], whose ground state is the paramagnetic insulator. For this model, the ground state for $U\to\infty$ is the highly degenerate set of total singlet states ($\sum_{i=1}^{N}S_i^z=0$).

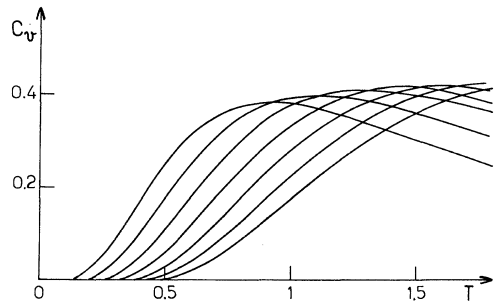

FIG. 15. Specific heat vs temperature of the paramagnetic solution in the insulating regime, for $U=4, 5, 6, \ldots, 10$.

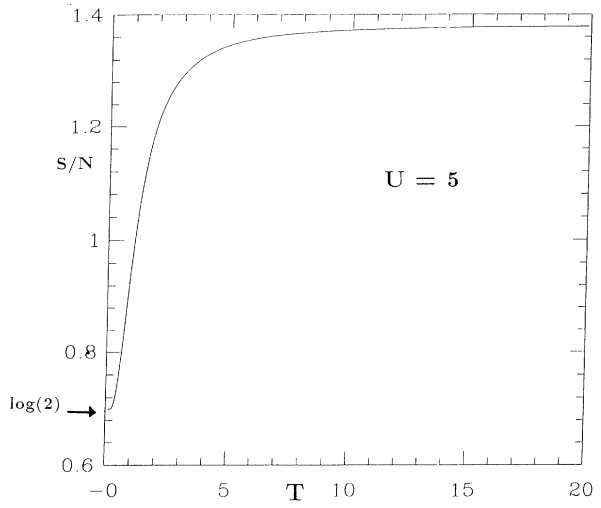

FIG. 16. Entropy per lattice site, S/N vs temperature, for $U=5$. Note the residual entropy $\sim \ln 2$ at $T=0$.

Note, furthermore, that the uniform magnetic susceptibility of the localized phase is finite and set by the $O(1)$ exchange scale. This is clearly seen in the numerical results of Fig. 12 for $U=4$. As a final evidence that the $d \to \infty$ limit does include charge fluctuations, we emphasize that the results of Fig. 6 for the fraction of doubly occupied sites show that $\langle D \rangle$ does not vanish even at zero temperature in this phase (as it would in the Gutzwiller approximation). Obviously, $\langle D(T=0) \rangle$ is not an order parameter of the Mott transition. We also notice that the $\langle D \rangle$ vs T curves do not seem to display a minimum for $U > U_c$, in contrast to the metallic phase. (For $U=4$, we have performed simulations down to $\beta=32$, without observing a minimum.) This is in agreement with the spin-entropy interpretation of this minimum given in Sec. V A.

D. Impurity-model interpretation

The localized phase has a simple interpretation in the impurity-model framework. Clearly, the effective conduction bath DOS $\Delta(\omega)$ itself develops a gap (or a pseudogap for the hypercubic lattice). The situation is analogous to a magnetic impurity in an insulator. The Kondo effect does not take place in that case, since no conduction states are present near $\omega=0$. The Kondo quasiparticle peak is absent, and the special density has a gap. In a renormalization-group picture, this situation corresponds to a flow towards *weak* Kondo coupling ($\sim t_*^2/U$), i.e., towards large U (or small hopping t_*). Hence, a local moment remains down to zero temperature. A simple argument can be given[9,10] which shows that the Fermi-liquid regime of the paramagnetic solution must indeed be unstable at large enough values of U. We imagine solving the impurity model iteratively, as in our algorithm. At the nth step of the iteration, $G_0^{(n)}$ is characterized by the spectral density $\Delta^{(n)}(\omega)$, which possibly has $\Delta^{(n)}(0) \neq 0$ and a nonzero width $W^{(n)}$ around $\omega=0$. In the first step of the algorithm, the impurity model is solved given $\Delta^{(n)}(\omega)$ to yield a local spectral density $\rho^{(n+1)}(\omega)$. The quasiparticle peak in $\rho^{(n+1)}$ has a width $T_K(W^{(n)}, U)$ (Kondo temperature) which is a function of U and of the width of $\Delta^{(n)}$. In the second step of the iteration, the self-consistency condition is used to produce an updated $\Delta^{(n+1)}$, which reads (for the Bethe lattice) $\Delta^{(n+1)}=t_*^2\rho^{(n+1)}/2$. Hence, the new width $W^{(n+1)}$ is essentially given by $T_K(W^{(n)}, U)$. Thus, when U is large, $W^{(n)}$ is *decreased upon iteration,* and one quickly reaches a regime in which it becomes smaller than the other energy scales. Using the relevant expression for $T_K(W, U)$ in this regime obtained by Haldane's renormalization-group analysis,[48] one gets

$$W^{(n+1)} \simeq W^{(n)} \sqrt{\Delta(0)/U}\, \exp[-U/\Delta(0)] \ .$$

Hence, for U large enough, $W^{(n)}$ is decreased at each step of the iteration and must converge to $W^{(\infty)}=0$. This signals the opening of a gap in $\Delta(\epsilon)$, and shows that the Fermi-liquid phase is indeed unstable for U very large.

E. Nature of the Mott transition

As explained in Sec. IV, an insulating solution of the paramagnetic equations in the IPT approximation exists for $U > U_{c1}$, while a metallic solution exists[11] for $U < U_{c2}$, with $U_{c1} < U_{c2}$, at $T=0$. The physical mechanism responsible for these two transitions are quite different. At U_{c2},[49] the quasiparticle residue $Z \simeq T_K$ vanishes continuously, hence destroying the coherence of the metal. This transition follows to some extent the Brinkman-Rice (BR) scenario,[47,36,37] with a diverging effective mass $m^*/m = 1/Z$. The *uniform* magnetic susceptibility does not diverge, however (hence the Wilson ratio *vanishes*), in contrast to the BR description which neglects exchange and charge fluctuation effects. Note that the BR value for U_{c2} (based on the Gutzwiller approximation) reads $U_{\rm BR}=8\epsilon_0 \simeq 4.5 t_*$ ($\simeq 4.8 t_*$ for the Bethe lattice), close to the value found within IPT.[11] Moreover, the Gutzwiller result for the quasiparticle residue $Z=1-U/U_{\rm BR}$ is not a bad description of the results of Fig. 8.

However, within IPT this continuous transition is preempted by the appearance of an insulating solution for $U > U_{c1}$, with $U_{c1} < U_{c2}$. This is quite unrelated to low-frequency coherence effects, but rather is a high-energy effect. It is due to the existence, at large enough U, of two degenerate magnetic solutions of the impurity problem at the Hartree-Fock level. The Mott insulating state is built from an incoherent superposition of these solutions. The insulating gap closes continuously at U_{c1}. This transition is qualitatively similar to the rigid-band picture of the Hubbard III approximation.

It results from the above that a region of coexistence is found in the (U, T) parameter space (Fig. 2) and that the Mott transition is found to be first order within IPT (see also Ref. 11). We find within IPT, at all temperatures that we studied ($T > 0.01$), that the insulating solution has lower free energy (due to the residual entropy $\simeq N \ln 2$), even though the internal energies are quite close. The actual critical line $U_c(T)$ is thus very close to the lower boundary of the coexistence region (Fig. 2).

VII. THE ANTIFERROMAGNETIC PHASE

In Secs. V and VI, we have described the behavior of the solution of the paramagnetic equations (5) and (6). On bipartite lattices, this corresponds to the actual equilibrium state of the model only for large enough temperatures. When the full set of equations (11) is solved, allowing for spin and translational symmetry breaking, the numerical results do converge towards the paramagnetic solution above the Néel temperature $T_N(U)$,[46] while a solution with long-range antiferromagnetic order is found for $T<T_N$. In Fig. 17 we show results obtained by exact enumeration ($L=16$) for the Green's functions on the hc lattice with $U=2.5$, $\beta=8$ [note that $G_{A,\sigma}(\tau)=G_{\beta,-\sigma}(\beta-\tau)$ at half filling]. Using this full algorithm, the Néel temperature can be calculated as a function of U together with the staggered magnetization in the antiferromagnetic phase from

$$m_s=\langle n_{\uparrow,A}-n_{\downarrow,A}\rangle=1+2G_{\uparrow,A}(\tau=0^+)\ .$$

We have calculated the Néel temperature as a function of U from both an extrapolation of $m_s(T)$ and the test of local stability of the paramagnetic solution.[45] The results were given on the phase diagram of Fig. 2 (Sec. IV): $T_N(U)$ is a maximum for $U\simeq 3$ and never exceeds ~ 0.14.

Figure 18 displays the staggered magnetization as a function of temperature for $U=2.5$ on the hc lattice. We find the Néel temperature to be $T_N(U=2.5)=0.13\pm 0.01$. This value agrees very well with Ref. 8, obtained by a different method based on the calculation of the staggered susceptibility. It was also noticed in Ref. 8 that recent Monte Carlo results for the $d=3$ case agree quite well with the $d\to\infty$ limit.

We have also investigated the IPT approximation in the antiferromagnetic phase: a comparison is made in Fig. 17. The agreement with the numerical solution is, by

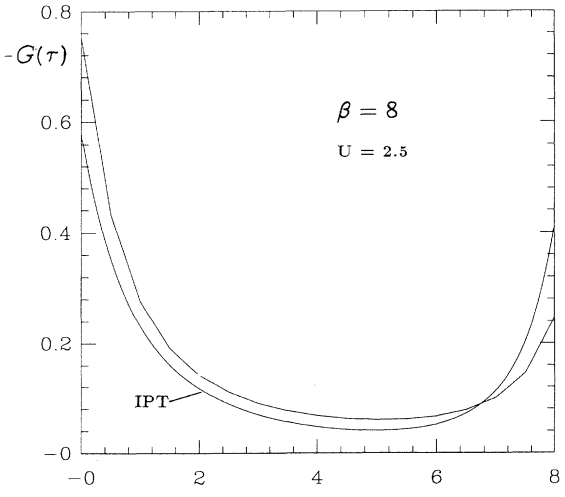

FIG. 17. Local Green's function $G_{A,\uparrow}(\tau)$ in the antiferromagnetic phase at $\beta=8$, $U=2.5$ (hc lattice). Upper curve: exact enumeration results. Lower curve: IPT approximation. Note that the latter underestimates m_s.

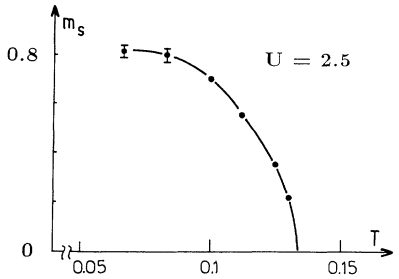

FIG. 18. Staggered magnetization m_s vs temperature at $U=2.5$.

far, not as good as in the paramagnetic case. The overall behavior of the Green's functions is qualitatively correct and the Néel temperature well approximated, but the staggered magnetization is not.

Finally, we have also determined the specific heat in the antiferromagnetic phase as a function of temperature. We find an activated behavior at low temperature, $\sim e^{-\Delta/T}$. This is expected from the fact that $d\to\infty$ is a mean-field limit in which spin-wave excitations are suppressed. Accordingly, C_v becomes very large close to T_N, and has a discontinuity at T_N. Above this discontinuity, the results of Figs. 4 and 15 are recovered. The large discontinuity is such that both the paramagnetic and antiferromagnetic solutions have the same integrated value for the entropy at T_N.

VIII. CONCLUSION

We have presented in this paper a detailed study of the physical properties of the $d=\infty$ Hubbard model at half filling, using a previously introduced numerical method to solve the exact mean-field equations satisfied by the Green's functions in this limit. Two equilibrium phases are found: a two-sublattice antiferromagnet at low temperature and a paramagnetic phase. In addition, the paramagnetic equations display a phase transition between a paramagnetic metal (Fermi liquid) for weak coupling and a paramagnetic Mott-Hubbard insulator for strong coupling. This transition can also be seen as a true ground-state phase transition for a fully connected Hubbard model with randomness on the hopping parameters.[31]

The nature of this transition within IPT is found to be more complex than suggested by many other approximate descriptions such as the Brinkman-Rice[47] and Hubbard approximations. We find (see also Ref. 11) a region of coupling and temperature in which two solutions of the mean-field equations coexist, from which we infer the existence of a first-order transition line extending to low but finite temperature. Both charge and spin *local* fluctuations are retained in the $d=\infty$ limit. As a result, we find no divergence of the *uniform* magnetic susceptibility at the transition and in the insulating phase, and no tendency to metamagnetism. The insulating phase does correspond, however, to the formation of local moments, and has (for $d=\infty$) a residual ground-state entropy. The IPT scenario of a first-order transition remains to be

verified in the full numerical solution of the mean-field equations.

We have also presented numerical results for several thermodynamic quantities (specific heat, entropy, density of doubly occupied sites) as a function of temperature. In the metallic regime, the results reflect the gradual separation of two energy scales: a low-energy scale associated with local spin fluctuations (corresponding to the Kondo scale in the associated single-impurity model) and a high-energy scale associated with charge fluctuations. The first scale disappears in the Mott insulator.

Finally, we have shown that a numerical solution of the $d=\infty$ Hubbard model can also be achieved within the long-range-ordered antiferromagnetic phase, and have presented results for the staggered magnetization as a function of temperature.

All these results demonstrate that a detailed quantitative understanding of strongly correlated fermion models can be achieved in the limit of infinite spatial dimensionality. The crucial physics of local spin and charge fluctuations is kept in this limit, leading to a rich variety of physical behavior. We believe that direct extensions of the present work may improve our understanding of physical systems such as liquid ^{3}He and Mott insulators. Other strongly correlated fermion models, such as the Kondo and Anderson lattices, are currently under investigation using the same methods. $d=\infty$ is also, in a sense, the simplest of all dimensions for the numerical study of fermionic lattice problems, since the problem is reduced to the solution of a self-consistent single-impurity model with no spatial degrees of freedom.

The $d=\infty$ limit does have some limitations however. In our opinion, the main one is the complete freezing of long-wavelength *spatial* fluctuations (such as, e.g., spin-wave modes), in contrast to *temporal* fluctuations which are treated exactly. It would be extremely interesting to find a theoretical scheme to include these fluctuations into the present framework, such as some kind of loop expansion around $d=\infty$.

ACKNOWLEDGMENTS

We would like to thank G. Kotliar, S. Sachdev, P. Nozieres, and D. S. Fisher for contributing very helpful remarks. We are also indebted to J. P. Bouchaud, J. K. Freericks, F. D. M. Haldane, M. Rozenberg, Q. Si, and X. Y. Zhang for interesting discussions. A.G. would like to thank G. Kotliar for collaboration and sharing many insights, and acknowledges the hospitality of Rutgers University, the Institute for Theoretical Physics in Santa Barbara (under NSF Grant No. PHY89-04035), and the International Center for Theoretical Physics in Trieste at various stages of this work. We recently received a copy of unpublished work by Pruschke *et al.*[50] which has some overlap with the present results and also investigates transport properties. Laboratoire de Physique Théorique is Unité propre du CNRS (UP 701) associée à l'ENS et à l'Université Paris-Sud. Laboratoire de Physique Statistique is Laboratoire associé au CNRS (URA 1306) et aux Universités Paris VI et Paris.

*Electronic address: GEORGES@PHYSIQUE.ENS.FR
†Electronic address: KRAUTH@PHYSIQUE.ENS.FR

[1]W. Metzner and D. Vollhardt, Phys. Rev. Lett. **62**, 324 (1989).
[2]For a recent review and references, see, e.g., D. Vollhardt, in *Correlated Electron Systems,* Proceedings of the Jerusalem Winter School of Theoretical Physics, edited by V. J. Emery (World Scientific, Singapore, in press).
[3]A. Georges and G. Kotliar, Phys. Rev. B **45**, 6479 (1992).
[4]A. Georges, G. Kotliar, and Q. Si, Int. J. Mod. Phys. B **6**, 705 (1992).
[5]P. van Dongen and D. Vollhardt, Phys. Rev. Lett. **65**, 1663 (1990).
[6]V. Janis, Z. Phys. B **83**, 227 (1991).
[7]The first detailed study of these mean-field equations was performed by U. Brandt and C. Mielsch, Z. Phys. B **75**, 365 (1989); **79**, 295 (1990); **82**, 37 (1991), in the restricted case $t_\uparrow \neq t_\downarrow = 0$ (Falicov-Kimball model), for which an exact solution is possible.
[8]M. Jarrell, Phys. Rev. Lett. **69**, 168 (1992); M. Jarrell and T. Pruschke (unpublished).
[9]A. Georges and W. Krauth, Phys. Rev. Lett. **69**, 1240 (1992).
[10]M. Rozenberg, X. Y. Zhang, and G. Kotliar, Phys. Rev. Lett. **69**, 1236 (1992).
[11]X. Y. Zhang, M. Rozenberg, and G. Kotliar, Phys. Rev. Lett. **70**, 1666 (1993); and (unpublished).
[12]J. Hubbard, Proc. R. Soc. London Ser. A **276**, 238 (1963).
[13]E. Muller-Hartmann, Z. Phys. B **74**, 507 (1989).
[14]They can, however, be considered as a mean-field *approximation* in more general instances, with an arbitrary DOS $D(\epsilon)$: it amounts to ignoring momentum conservation in all *skeleton* diagrams for the self-energy, while retaining frequency conservation.
[15]A useful numerical algorithm for the complex error function has been published as "algorithm 680, collected algorithms from ACM," [Transact. Math. Software **16**(1), 47]. We are grateful to J. K. Freericks for pointing this out to us.
[16]B. Horvatic and V. Zlatic, Solid State Commun. **75**, 263 (1990).
[17]See, e.g., A. L. Fetter and J. D. Walecka, *Quantum Theory of Many-Particle Systems* (McGraw-Hill, New York, 1971). As written, this formula is particularly well suited to deal with numerical frequency summations since all terms decay faster than $1/\omega$.
[18]P. W. Anderson, Phys. Rev. **124**, 41 (1961).
[19]P. A. Wolf, Phys. Rev. **124**, 1030 (1961).
[20]In actual computations, we take for $G(i\omega_n)$ the Fourier transform of a function constructed from the points $G(\tau_l)$ by a spline interpolation and such that it has the correct amplitude of the jump at $\tau=0$: $G(\tau=0^+)-G(\tau=0^-)=-1$.
[21]G_0 is self-consistently determined and does not have, in general, the form corresponding to the integrable case for the impurity model, except for a very special (Lorentzian) choice of the DOS $D(\epsilon)$, which has rather nongeneric properties: see Refs. 3 and 4.
[22]J. E. Hirsch and R. M. Fye, Phys Rev. Lett. **56**, 2521 (1986).
[23]R. Blankenbekler, D. J. Scalapino, and R. L. Sugar, Phys. Rev. D **24**, 2278 (1981).
[24]The enumeration proceeds as $(\cdots -1,-1,-1,-1)$, $(\cdots -1,-1,-1,+1)$, $(\cdots -1,-1,+1,+1)$, $(\cdots -1,-1,+1,-1)$, etc. See E. M. Reingold, J. Niever-

gelt, and N. Deo, *Combinatorial Algorithms, Theory and Practice* (Prentice Hall, Englewood Cliffs, NJ, 1977).

[25]H. J. Vidberg and J. W. Serene, J. Low Temp. Phys. **29**, 179 (1977).

[26]The final results for physical quantities are obtained by extrapolating to small $\Delta\tau(L\to\infty)$. For the range of parameters studied, this turned out to be safely possible provided $\Delta\tau$'s of order 0.5 are reached.

[27]K. Yosida and K. Yamada, Prog. Theor. Phys. **46**, 244 (1970); **53**, 1286 (1975); K. Yamada, *ibid.* **53**, 970 (1975); V. Zlatic, B. Horvatic, and D. Sokvecic, Z. Phys. B **59**, 151 (1985); M. Salomaa, Solid State Commun. **39**, 1105 (1981).

[28]H. Schweitzer and G. Czycholl, Z. Phys. B **83**, 93 (1991).

[29]E. Muller-Hartmann, Z. Phys. B **76**, 211 (1989).

[30]B. Menge and E. Muller-Hartmann, Z. Phys. B **82**, 237 (1991).

[31]This has been established in a joint work with S. Sachdev. We are also indebted to D. S. Fisher for very useful remarks on this point.

[32]Note that this fully connected model can be solved analytically in the absence of randomness, see P. Van Dongen and D. Vollhardt, Phys. Rev. B **40**, 7252 (1989).

[33]More precisely, denoting by $E(\beta,L)$ the internal energy for a given inverse temperature and grid size, we compute C_v as $C_v(\beta=L\Delta\tau,\Delta\tau)=E(L\Delta\tau,L)-E[(L+1)\Delta\tau,L+1]/(L\Delta\tau)^{-1}-[(L+1)\Delta\tau]^{-1}$, and extrapolate for $\Delta\tau\to 0$.

[34]D. S. Greywall, Phys. Rev. B **27**, 2747 (1983).

[35]K. Seiler, C. Gros, T. M. Rice, K. Ueda, and D. Vollhardt, J. Low Temp. Phys. **64**, 195 (1986).

[36]D. Vollhardt, Rev. Mod. Phys. **56**, 99 (1984).

[37]See, e.g., P. Nozieres (unpublished).

[38]D. B. McWhan, J. P. Remeika, T. M. Rice, W. F. Brinkman, J. P. Maita, and A. Menth, Phys. Rev. Lett. **27**, 941 (1971).

[39]D. Langreth, Phys. Rev. **150**, 516 (1966).

[40]P. Nozieres, J. Low Temp. Phys. **17**, 13 (1975).

[41]A. Fujimori, I. Hase, H. Namatame, Y. Fujishima, Y. Tokura, H. Eisaki, S. Uchida, K. Takegahara, and F. M. F. de Groot, Phys. Rev. Lett. **69**, 1796 (1992).

[42]S. Wiegers, P. E. Wolf, and L. Puech, Phys. Rev. Lett. **66**, 2895 (1991).

[43]J. Hubbard, Proc. R. Soc. London Ser. A **281**, 401 (1964).

[44]We thank D. S. Fisher and P. Nozieres for clarifying discussions on this point.

[45]The convergence is slow close to T_N, and can be sped up tremendously using standard methods of acceleration of slowly converging series. We have used the Shanks transform described in C. M. Bender and S. A. Orszag, *Advanced Mathematical Methods for Scientists and Engineers* (McGraw-Hill, New York, 1978), p. 396 ff.

[46]For some values of U, T, a modified update formula has been used in order to avoid cycles in the algorithm, e.g., $G_{0,\text{new}}=1/2[G_0+\tilde{D}(i\omega_n-\Sigma)]$.

[47]W. F. Brinkman and T. M. Rice, Phys. Rev. B **2**, 4302 (1970).

[48]F. D. M. Haldane, Phys. Rev. Lett. **40**, 416 (1978); Ph.D. thesis, University of Cambridge, 1977 (unpublished).

[49]For recent analytic insights into this transition, see Ref. 11 and D. S. Fisher (unpublished).

[50]T. H. Pruschke, D. L. Cox, and M. Jarrell (unpublished).